All optical method for investigation of spin and charge transport in semiconductors: Combination of spatially and time-resolved luminescence

F. Cadiz, P. Barate, D. Paget, D. Grebenkov, J. P. Korb, A. C. H. Rowe, T. Amand, S. Arscott, and E. Peytavit

Citation: Journal of Applied Physics **116**, 023711 (2014); doi: 10.1063/1.4889799
View online: http://dx.doi.org/10.1063/1.4889799
View Table of Contents: http://scitation.aip.org/content/aip/journal/jap/116/2?ver=pdfcov
Published by the AIP Publishing

All optical method for investigation of spin and charge transport in semiconductors: Combination of spatially and time-resolved luminescence

F. Cadiz,[1] P. Barate,[2] D. Paget,[1] D. Grebenkov,[1] J. P. Korb,[1] A. C. H. Rowe,[1] T. Amand,[2] S. Arscott,[3] and E. Peytavit[3]
[1]*Physique de la matière condensée, Ecole Polytechnique, CNRS, 91128 Palaiseau, France*
[2]*Université de Toulouse, INSA-CNRS-UPS, 31077 Toulouse Cedex, France*
[3]*Institut d'Electronique, de Microélectronique et de Nanotechnologie (IEMN), University of Lille, CNRS, Avenue Poincaré, Cité Scientifique, 59652 Villeneuve d'Ascq, France*

(Received 12 May 2014; accepted 27 June 2014; published online 14 July 2014)

A new approach is demonstrated for investigating charge and spin diffusion as well as surface and bulk recombination in unpassivated doped semiconductors. This approach consists in using two complementary, conceptually related, techniques, which are time-resolved photoluminescence (TRPL) and spatially resolved microluminescence (μPL) and is applied here to p^+ GaAs. Analysis of the sole TRPL signal is limited by the finite risetime. On the other hand, it is shown that joint TRPL and μPL can be used to determine the diffusion constant, the bulk recombination time, and the spin relaxation time. As an illustration, the temperature variation of these quantities is investigated for p^+ GaAs. © *2014 AIP Publishing LLC*. [http://dx.doi.org/10.1063/1.4889799]

I. INTRODUCTION

Determination of diffusion constants and characterization of surface and bulk recombination of semiconductors is of importance for the designing of devices, such as photovoltaic, microelectronic, and spintronics systems. The diffusion constants are usually obtained from the values of minority carrier mobilities.[1–3] The charge and spin diffusion constants can also be determined using spin grating experiments.[4] In spite of their strong interest, these experiments are relatively elaborate since they involve time-resolved four-wave mixing. For determination of the recombination dynamics, time-resolved photoluminescence (TRPL),[5] cathodoluminescence,[6,7] or conductivity[8] have been used. Independent theoretical analysis[9,10] has shown the strong potential of time-resolved techniques for investigating bulk and surface recombination, and for the determination of diffusion constants using analysis of the various exponential modes in the transient, for each of which the characteristic time and amplitude can, in principle, be determined independently. Such analysis has only been performed for silicon.[8] Experiments on p^+ GaAs have investigated bulk[11] and to some extent surface[12] recombination kinetics, as well as spin and charge lifetimes.[13–15] Both time and spatially resolved luminescence has also been used for investigating minority carrier and transport in surface free n-type GaAs.[16]

In the present work, it is first shown, in the case of doped unpassivated GaAs, that analysis of the charge and spin transients can be performed using an inverse Laplace transform method, which gives well-defined temporal modes. However, the finite TRPL rise time only enables to observe the first two modes, while their amplitudes are difficult to determine. On the other hand, the joint use of TRPL and of spatially resolved microphotoluminescence (μPL) enables to determine the charge and spin lifetimes as well as the charge and spin diffusion constants. The μPL technique, which consists in imaging the photoluminescence profile using a local CW laser excitation,[17] is formerly very similar to TRPL since the spatial concentration profile also exhibits modes. This method is applied to investigation of the temperature dependences of diffusion constant, lifetime, spin relaxation time for p^+ GaAs, for which the interest for spintronics arises from the strong electronic polarization under circularly polarized excitation. Section II presents a description of the method with an illustration at low temperature and shows the conceptual analogies of the two techniques. Section III presents a discussion of the limits of the sole TRPL and an interpretation of the joint TRPL and μPL results. In Sec. IV, the method is applied to investigation of temperature effects and spectrally dependent dynamic characteristics.

II. DESCRIPTION OF THE METHOD

A. Experimental

We have investigated a thin GaAs film (acceptor concentration $N_A = 10^{18}\,\mathrm{cm}^{-3}$, thickness $d = 3\,\mu\mathrm{m}$). This structure is grown on a GaInP layer, which is itself grown on a semi-insulating substrate which does not contribute to the luminescence. The thin GaInP layer confines the photoelectrons and also strongly reduces the recombination at the back film interface. The present section is devoted to results obtained at a temperature near 15 K, while the results as a function of T will be explained in Sec. IV.

For TRPL, as described in Ref. 18, the excitation source was a circularly polarized mode-locked frequency-doubled Ti:Sa laser (1.5 ps pulse width, 80 MHz repetition frequency, wavelength 780 nm) and the emitted light was dispersed by a spectrometer (resolution 0.12 nm) and detected by a streak camera. The average power was adjusted between 5 and 500 μW and the diameter of the excitation spot was 50 μm that is, much larger than the diffusion length, so that light excitation was spatially homogeneous. The spin-related

difference signal $I_d(t) = I_+(t) - I_-(t)$, defined as the difference between the σ^+- and σ^--polarized components of the transient luminescence signal was also monitored. Figure 1 shows the sum and difference transients obtained at 20 K normalized to unity at their maximum as well as, for comparison, the time response of the streak camera. These transients reveal a slow increase, in a time of the order of 70 ps, an exponential tail at long times, and a relatively weak nonexponential signal between 100 ps and 300 ps, and will be interpreted in Sec. III B.

For μPL, as described in Ref. 17 and illustrated in the left panel of Fig. 2, the sample was excited by a CW tightly focused light (Gaussian radius $\sigma \approx 0.6\,\mu$m, energy 1.59 eV) in a modified commercial optical microscope. An image of the luminescence was taken using a CCD camera and a small light excitation power (several μW) in order to keep a photoelectron concentration smaller than $10^{16}\,\mathrm{cm}^{-3}$ and to avoid effects of ambipolar diffusion[19] and of Pauli blockade.[20] Such image, at a temperature of 15 K, is shown in the top right panel of Fig. 2. The bottom right panel shows the angular averaged sum profile. This profile is distinct from that of the laser and reveals photoelectron diffusion during their lifetime.

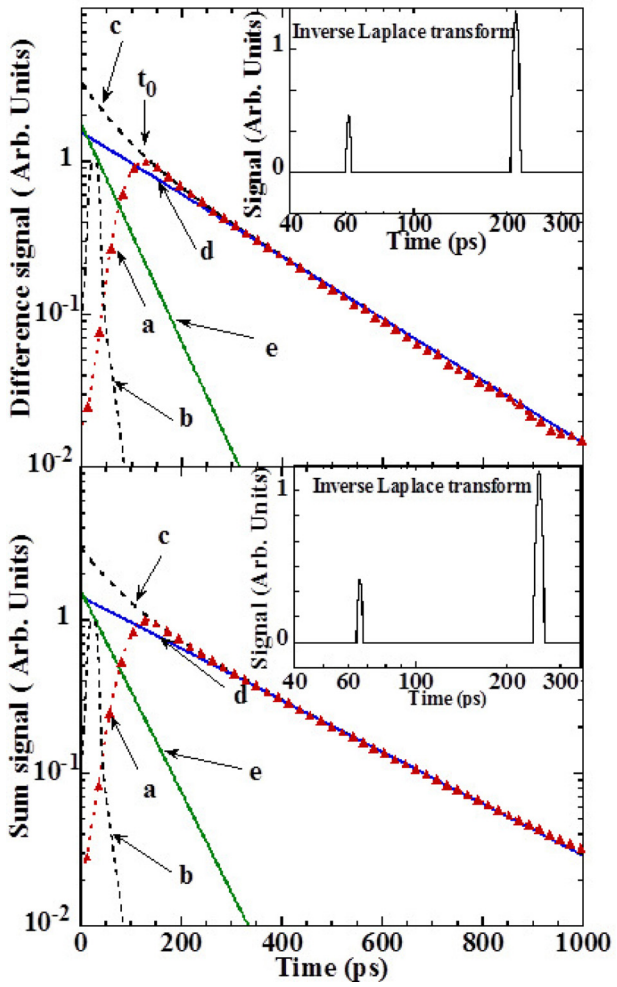

FIG. 1. Sum (bottom panel) and difference (top panel) TRPL signals and their analysis, taking the time of the excitation pulse at the time origin. Curves *a* show the measured sum and difference transients at 20 K, normalized at their maximum, and curves *b* show for comparison the detector time response. The inset reveals two exponential decay modes and gives their characteristic times and weights. The sum of these exponentials, shown in curves *c*, gives a very good approximation to the decay signal at times larger than about 100 ps after the laser pulse. These exponentials are shown individually in curves *d* and *e*.

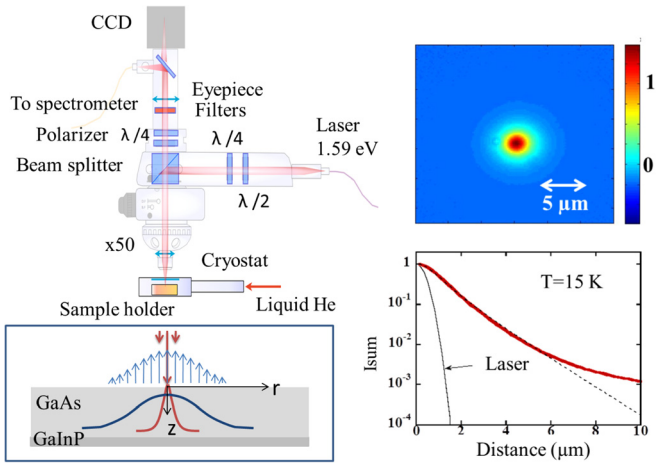

FIG. 2. Microphotoluminescence. The left panel shows the principle of the μPL technique, in which a laser is tightly focused onto the sample, and where an image (shown in the top right panel) is taken using a CCD camera. The bottom right panel shows an angular-integrated section of this image in the same conditions as Fig. 1, together with a fit and the cross section of the laser profile.

B. Theory

For the two techniques, the luminescence intensity is given by

$$I = C\int_0^d e^{-\alpha_l z} n(r,z,t)dz, \tag{1}$$

where C is a constant. Here, t is the time and, as shown in the left panel of Fig. 2, r is the distance to the excitation spot and z is the depth. This equation allows for the possibility of reabsorption of the luminescence with a coefficient α_l. The photoelectron concentration $n(r, z, t)$ is a solution of the following diffusion equation:

$$\frac{\partial n(r,z,t)}{\partial t} = g(r,z,t) - \frac{n(r,z,t)}{\tau} + D\Delta n(r,z,t), \tag{2}$$

where D is the charge diffusion constant, τ is the bulk lifetime, and Δ is the Laplacian operator. Here, $g(r, z, t)$ is the number of thermalized electrons created in the conduction band per unit volume and per unit time and takes into account the possible spatial diffusion of hot electrons during thermalization. For μPL, one has $g(r,z,t) = g_\mu(r,z)$ so that, in Eq. (1), $\partial n(r, z, t)/\partial t = 0$. For TRPL, $g(r,z,t) = g_{TR}(z,t)$ so that $n(r, z,t)$ does not depend on r. Equation (2) is solved in Appendix by imposing the Robin boundary conditions $\partial n/\partial z|_{z=0} = \gamma n/d$ and $\partial n/\partial z|_{z=d} = -\gamma' n/d$, where the dimensionless parameters γ and γ' are related to the recombination velocities S and S' of the front and back surfaces, respectively, by

$$\gamma = \frac{Sd}{D} \quad \gamma' = \frac{S'd}{D}. \tag{3}$$

For TRPL, the difference signal $I_{dTR}(t)$ is also given by Eq. (1) provided the charge concentration n is replaced by the spin concentration $s = n_+ - n_-$, where $n_\pm$ is the concentration of electrons of spin $\pm 1/2$, with a quantization axis along the direction of light excitation. The quantity C is replaced by $C|\mathcal{P}_i|$ where, for cubic semiconductors, the initial polarization $\mathcal{P}_i$ is equal to ∓ 0.5 for $\sigma^\pm$-polarized light excitation. The time evolution of s is given by an equation similar to Eq. (2) where $g_{TR}(z,t)$ is replaced by $g_{TR}(z,t)\mathcal{P}_i$ and where τ is replaced by the spin lifetime $\tau_s = (1/\tau + 1/T_1)^{-1}$, where T_1 is the spin relaxation time. The spin diffusion constant D_s can be smaller than D if spin drag is present.[21] Within these changes, Eqs. (7), (A6), and (A3) also give the expression for $I_d(t)$, as a function of the characteristic times τ_{sm} of the various modes for the decay of s.

1. TRPL signal

For a time-dependent, spatially homogeneous, light excitation, the concentration is expressed as

$$n(z,t) = \sum_m a_m u_m(z) e^{-t/\tau_m}, \tag{4}$$

where a_m are functions of time and $u_m(z)$ are the orthogonal spatial eigenfunctions of the Laplacian operator, satisfying the above boundary conditions, and given by Eq. (A1).[5,22] The characteristic times τ_m of the various modes are given by

$$1/\tau_m = 1/\tau + D\theta_m^2/d^2, \tag{5}$$

where the angle θ_m is given by the nonlinear equation

$$\theta_m = \mathrm{Arctan}(\gamma/\theta_m) + \mathrm{Arctan}(\gamma'/\theta_m) + (m-1)\pi. \tag{6}$$

The final expression of the luminescence intensity, found using Eq. (1), is

$$I_{\mathrm{TR}}(t) = C\sum_m c_m e^{-t/\tau_m}, \tag{7}$$

where c_m are functions of time, given by Eq. (A3). In the simplified case where the buildup of the thermalized electron population is instantaneous, one has $g_{TR}(z,t) \propto \alpha\delta(t)e^{-\alpha z}$, where α is the absorption coefficient. The functions c_m are constants, $c_m = n_0 c_m^0$ where n_0 is proportional to the excitation power and c_m^0, given by Eq. (A4), only depends on γ and γ'. Assuming that $\gamma' = 0$, the dependences of c_m^0 on γ are illustrated in Fig. 3, neglecting photoluminescence reabsorption ($\alpha_l = 0$). For a passivated surface ($\gamma = 0$ which gives $c_1^0 = 1$), only one mode is present in the transient, of time equal to τ. If on the other hand S is not negligible, determination of c_m^0 gives γ and θ_m using Eq. (6). Provided more than one mode is observed, these angles, together with the measured values of τ_m, give D using Eq. (5) from which τ and S are obtained.[23]

2. μPL profile

For μPL, the spatially inhomogeneous rate of creation of thermalized electrons is approximated by $g_\mu(r,z) \propto \alpha^* e^{-\alpha^* z} e^{-(r/\sigma^*)^2}$, where σ^* and α^* can differ from the Gaussian radius σ of the laser spot and from the absorption coefficient α^*, respectively, because of hot electron diffusion. In analogy with Eq. (7) and, as shown in Appendix, the luminescence profile can be expressed as the sum of spatial modes as given by

$$I_{\mu PL}(r) \propto \sum_m c_m^0 \int_0^\infty K_0\left(\frac{r'}{L_m}\right) e^{-(r-r')^2/\sigma^{*2}} dr'. \tag{8}$$

The spatial mode of order m is proportional to the modified Bessel function of the second kind K_0 convoluted with the effective excitation profile and multiplied by the same amplitude c_m^0 as for TRPL. The mode of order m decays as a function of r with a characteristic distance

$$L_m = \sqrt{D\tau_m}, \tag{9}$$

which decreases with m. Modal analysis of the experimental spatial profile in principle gives the values of c_m^0 and L_m. However, such analysis requires a precise knowledge of σ^* and is generally not possible as soon as the kinetic energy of electrons at creation becomes significant.

As shown in the Appendix, the diffusion equation also has an analytical solution given by Eq. (A8), obtained using a treatment similar to Ref. 24. This solution is expressed as a function of S, S', and of the bulk diffusion length $L = \sqrt{D\tau}$. For the calculation of the profile, it is possible to take $S = S' = 0$ and $L = L_1$, which is equivalent to replacing in Eq. (8) all L_m by L_1. This implies that the profile essentially depends on one parameter, L_1.

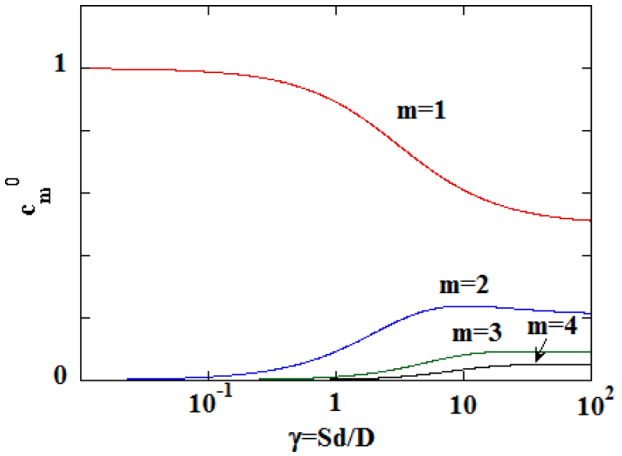

FIG. 3. Dependence of the amplitudes c_m^0 of the various modes defined in Eq. (7), calculated using Eq. (A4) and using in Eq. (1) $\alpha_l = 0$. For a passivated surface ($\gamma = 0$), only one mode is present in the transient, of time equal to τ.

III. INTERPRETATION

A. Analysis of the sole TRPL transient

A convenient method for the analysis of the decays in Fig. 1 is to choose as a time origin the time t_0 of the signal maximum and to perform an inverse Laplace transform, using a numerical resolution of the following 1D inverse Fredholm integral of the first kind

$$I_{TR}(t-t_0) = \int_{\tau_{min}}^{\tau_{max}} J(\tau) e^{-(t-t_0)/\tau} d\tau + \varepsilon(t), \qquad (10)$$

where $J(\tau)$ is the searched distribution of time constants, $\varepsilon(t)$ represents the noise. This algorithm is based on a compression of the data obtained with the singular value decomposition of the exponential kernel and a robust optimization method using a Tikhonov regularization.[25] Shown in the insets of Fig. 1 are the time-dependences of $J(\tau)$. Though the inverse Laplace transform is known as an ill-posed problem, the very good signal-to-noise ratio of the experimental data gives two well-defined peaks such that

$$I_{TR}(t-t_0) = c_1^* e^{-(t-t_0)/\tau_1} + (1-c_1^*) e^{-(t-t_0)/\tau_2}, \qquad (11)$$

where $\tau_1 = 256$ ps, $\tau_2 = 66$ ps, and $c_1^* = 0.82$. In the same way, the difference signal is described by $I_{dTR}(t-t_0) = c_{s1}^* e^{-(t-t_0)/\tau_{s1}} + (1-c_{s1}^*) e^{-(t-t_0)/\tau_{s2}}$, where $\tau_{s1} = 215$ ps, $\tau_{s2} = 63$ ps, $c_{s1}^* = 0.725$, and $t_0 = 140$ ps. Curves *d* and *e* of Fig. 1 show the individual exponential modes. The data are very well approximated by their sums (curves *c*).

The two successive exponential decays of Eq. (11) are attributed to the first two modes defined in Eq. (7). Other interpretations implying ambipolar diffusion,[19] Auger recombination at high density, change of recombination time caused by temperature dependence of the bimolecular recombination,[5,26,27] or stimulated emission by the photoexcited carriers, can be ruled out since the transient stays exactly the same if the excitation power is decreased by two orders of magnitude. In the same way, time dependence of the spin relaxation time, possibly originating from the concentration dependence of the collision time,[28] can be excluded because of the weak power dependence of the difference transient. Finally, transient dielectric screening of carriers can also be ruled out since the dielectric relaxation time is very short as compared to τ_2.[29]

The increase of the sum and difference signals masks the higher order modes. This slow increase has already been reported before for p^+ GaAs[14] and has been attributed to the screening of the electron-phonon interaction.[30] Nevertheless, since the amplitudes have well-defined, time-independent, values as soon as the PL maximum is reached, one may think that the experimentally determined ratio $c_1^*/(1-c_1^*)$ should be equal to c_1^0/c_2^0 and should allow us to determine γ as shown by Fig. 3. This is however not true since the signal increase cannot be interpreted by Eq. (A6) using a single time for thermalization of electrons after creation. In this case, the amplitude values, given by Eq. (A3), depend on details of the thermalization process, which are not known, such as (i) the change of the electron depth profile by diffusion during thermalization; (ii) the possible time dependence of τ induced by its temperature dependence.[5] In view of this complexity, it is concluded that only the times of the transients can be used for analysis, so that investigation of the PL sum and difference transients is not sufficient to determine intrinsic dynamic and diffusive parameters.

B. Combined TRPL and μPL investigation

As shown in the Appendix, the higher order spatial modes do not affect the μPL signal for distances larger than 2 μm. Thus, analysis of the profile at longer distances can be restricted to the lowest order mode of Eq. (8). This gives $L_1 = 1.33$ μm from which we find $D = 80 \pm 15\,\mathrm{cm^2/s}$ using Eq. (9).[31] Taking $S' = 0$ for simplicity, Eq. (6) becomes $\theta_1 \tan\theta_1 = \theta_2 \tan\theta_2$ and gives using Eq. (5) a nonlinear equation whose resolution gives $\tau = 270 \pm 50$ ps, $L = 1.46$ μm, and $S = 4.6 \times 10^4$ cm/s. However, since τ is very close to τ_1,[32] the uncertainty on the determination of S is very large, of at least one order of magnitude. The profile is finally calculated using Eq. (A8), using the above determined parameter values and $\sigma^* = 0.6$ μm. The result is shown as a dotted line in the bottom right panel of Fig. 2 and very well approximates the data. It is concluded that combination of TRPL and μPL allows us to determine the key parameters for recombination and transport.

Investigation of the spin dynamics is performed by calculating the transient of the spin polarization $\mathcal{P} = (n_+ - n_-)/(n_+ + n_-)$, defined as the ratio of the difference and sum transients. This transient is shown in Fig. 4, taking the time origin at $t_0 = 140$ ps in order to avoid the effects of the slow signal increase. As seen in the inset, the fast tail has almost completely disappeared and the transient is essentially described by a single exponential of characteristic time $T_1 \approx 1150$ ps. Using Eq. (7) and the corresponding equation for spin orientation, one can show that this result implies that $D_s \approx D$ so that, in Eq. (6), $\theta_1 = \theta_{1s}$ and $\theta_2 = \theta_{2s}$. The transients at short time calculated using Eq. (7) for several values of the ratio D_s/D are shown in the main figure along with the data. From the good agreement obtained for D_s/D near unity, we conclude that $D_s/D = 1 \pm 0.1$, in agreement with Ref. 21 for a similar doping. It is concluded that, if present, spin drag only marginally affects spin transport.

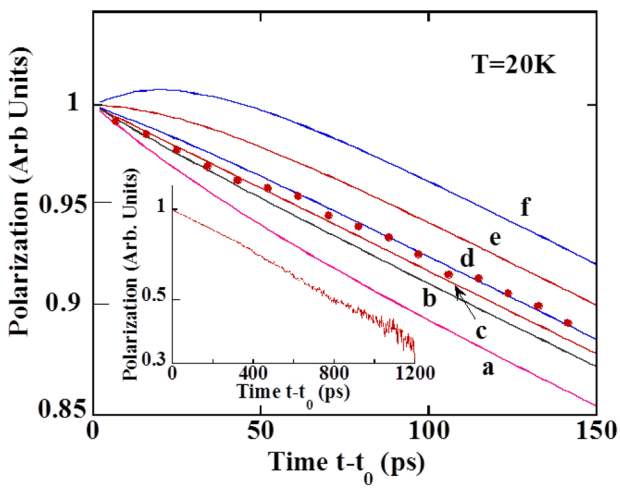

FIG. 4. Ratio of the spin to charge diffusion constants. The inset shows the light polarization transient, calculated from curves *b* of Fig. 5 and taking the time of the maximum t_0 as the time origin. This transient mostly exhibits a single exponential. The dots show the same transient at short times. The curves are calculated using Eq. (7) taking a ratio D_s/D of the spin to charge diffusion constants equal to 0.3 (a), 0.9 (b), 1 (c), 1.1 (d), 1.3 (e), and 1.5 (f). From the almost ideal exponential behavior of the transient, it is concluded that $D_s/D = 1 \pm 0.1$.

IV. DISCUSSION

A. Temperature effects

The analysis of Sec. III has also been performed as a function of temperature. As seen in the bottom panel of Fig. 5, which shows the sum TRPL signals, the decay time τ_1 at the long time increases with temperature. This shows that τ_1 is dominated by the decrease with temperature of the bulk recombination efficiency[5] rather than by the increase of surface recombination velocity. In agreement with Eq. (A4) and Fig. 3, the increase of S is responsible for the observed temperature increase of the amplitude of the fast exponential decrease before 400 ps. The top panel of Fig. 5 shows the temperature dependence of the difference signal. Up to about 80 K, the time τ_{s1} of the long time transient increases with temperature, in the same way as for the sum transient. Further temperature increase induces a decrease of τ_{s1}, which reveals a temperature decrease of the spin relaxation time T_1. The difference transient also exhibits a temperature increase of the amplitude of the short time transient. Such effect is caused by the increase with temperature of the surface recombination velocity, which will increase c_2 as shown in Fig. 3. Note also that, in agreement with independent observations,[14] the characteristic time for the increase of the two signals weakly depends on temperature. Also visible is the slow tail at very long times observed for the sum transient and to some extent for the difference transient at the lowest temperature of 10 K. This finding will be discussed in Sec. IV B.

The sum μPL profiles are also shown in Fig. 6 for selected temperatures. The spatial decay is slightly faster when the temperature is decreased, thus revealing a limited decrease of L_1. Also shown in the figure are the best fits of the experimental data using Eq. (A8) using $S = S' = 0$. The agreement with the experimental data is satisfactory. Table I gives the values of τ_1 and of τ_2, as obtained by inverse Laplace analysis, of L_1 as well as the resulting values of D and τ.

At room temperature, $D = \mu kT/q$, as defined by the Einstein relation, is close to the value of 50 cm ^{2}/s, calculated using a typical minority carrier mobility of 2000 cm^2/Vs.[1] The value of D only slightly increases with decreasing temperature, because of the approximate $1/T$ dependence of the mobility μ.[2] The difference between τ and τ_1 becomes visible at temperatures larger than about 100 K because in this temperature range, the surface recombination velocity starts to play a role. However, the value of τ at 300 K is smaller by a factor of 3 than the bulk radiative lifetime for the present acceptor concentration[11] and the temperature increase is characterized by an exponent of the order of 0.5 as a function of T and closer to 1 as a function of the temperature of the electron gas. These exponents are smaller than the one of 3/2 found for bulk radiative recombination.[5] These two differences are attributed to nonradiative recombination at the rear surface, for which the time decreases with increasing temperature. At room temperature, the characteristic time for the back surface recombination, of the order of $(S'/d)(\theta_1/\tan(\theta_1))$ provided $\gamma' \ll \gamma$, can be estimated using the value of $S' = 10^5$ cm/s found on a sample with a doping higher by one order of magnitude.[33] One finds a value slightly smaller than 1 ns, showing that back surface recombination could affect the value of τ. Finally, the fact that τ is not larger than its expected value for radiative recombination suggests that photon recycling effects are weak. Such recycling would result in an increase of τ and is indeed expected to be small in the presence of a substrate.[34]

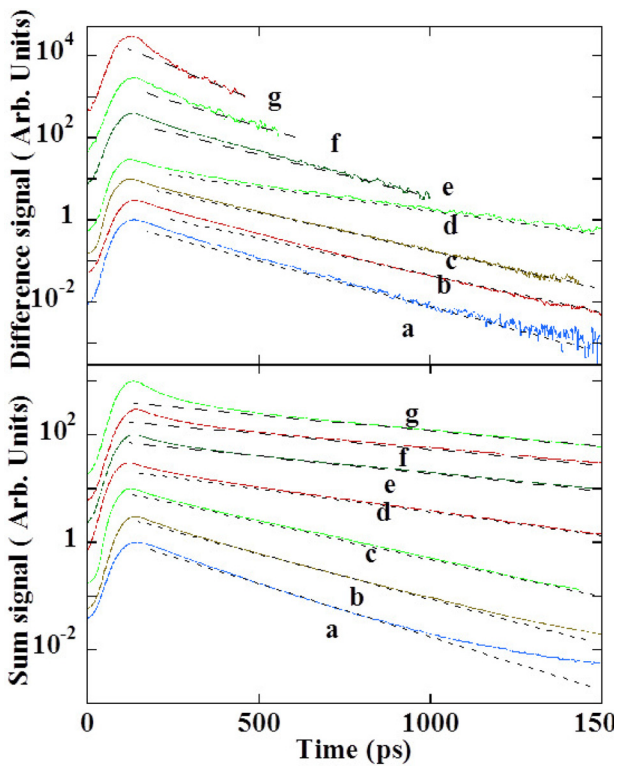

FIG. 5. Temperature effects investigated using TRPL. The bottom panel shows the experimentally observed transient sum signals observed for selected lattice temperatures of 10 K (a), 20 K (b), 40 K (c), 80 K (d), 150 K (e), 225 K (f), and 300 K (g). The curves were normalized and shifted upwards for clarity and regions of small signal-to-noise have been omitted for clarity. The top panel shows the corresponding difference transients.

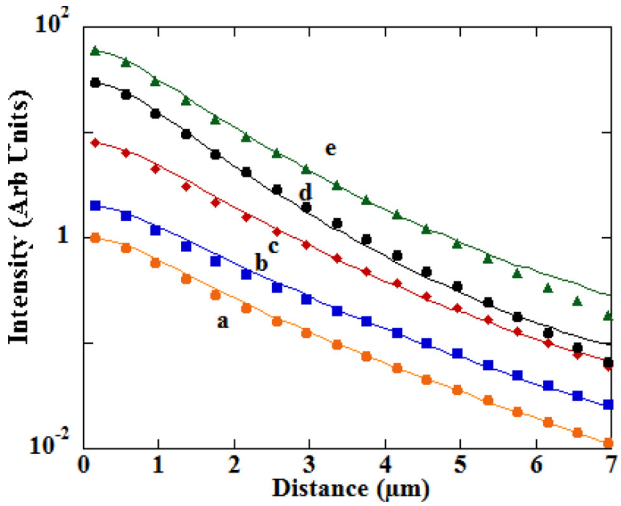

FIG. 6. Temperature effects investigated using μPL. Experimental spatial decay of the luminescence intensity as a function of distance to the laser excitation spot, for selected lattice temperatures of 300 K (a), 80 K (b), 40 K (c), 15 K (d), and 8 K (e). The curves, normalized at the maximum, were shifted upwards for clarity. Also shown by dots are curves calculated using Eq. (A8), using an effective diffusion length given in Table I.

TABLE I. Values of effective diffusion length of the characteristic times of the first two TRPL modes and of the calculated charge diffusion constant and bulk recombination time for selected temperatures. Values in parentheses in the first line give uncertainties.[32]

T	L_1 (μm)	τ_1 (ps)	τ_2 (ps)	D (cm^2/s)	τ (ps)
9	1.45(0.05)	189(10)	51(10)	111(15)	261(50)
15	1.33	256	60	80	268
40	1.80	319	69	101	319
80	2.10	524	106	84	546
150	2.11	717	93	62	944
225	2.28	796	95	67	871
300	2.02	717	90	57	1097

Analysis of the dependence of T_1 as a function of lattice temperature as well as of the photoelectron temperature T_e, as determined from the shape of the PL spectrum, is shown in Fig. 7. A power law is found for the two curves with exponents of 1.16 and of 1.41 as a function of T and T_e, respectively. The latter exponent is very close to that found using Hanle effect measurements for a similar doping,[34] which shows the relevance of the exchange interaction of the electronic spins with the hole spins (known as the Bir Aronov Pikus mechanism).[5]

B. Energy-resolved analysis at $T = 9$ K

In the present section, we apply analysis of the TRPL signal to spectroscopic investigation as a function of luminescence energy. Unlike higher temperatures, the transient at $T = 9$ K depends on energy. The luminescence spectra at 9 K for selected times after the laser pulse are shown in the bottom panel of Fig. 8. While the spectrum shape does not strongly change during the signal increase, the spectrum after the onset of the decrease exhibits a stronger high energy signal (above 1.5 eV) and a relatively weak signal at an energy lower than 1.49 eV. Conversely, at long times, the luminescence peaks at a lower energy of 1.492 eV, implying an energy-dependent recombination time τ_1. The value of τ_1, determined using inverse Laplace analysis [Eq. (10)], is shown in the inset of Fig. 8 as a function of energy and is larger at low energy. Such behavior is well-known in disordered systems at low temperatures and indicates photoelectron localization in potential wells caused by the random distribution of acceptors.[35] Although at this acceptor concentration the holes remain delocalized,[36] the electron localization decreases the overlap between electron and hole wave functions, which explains the lifetime increase.

The light polarization spectra at selected times after the laser pulse, shown in the top panel of Fig. 8, exhibit the progressive build up a polarization dip near 1.49 eV. This implies that, both for electrons of higher and lower energy, the lifetime τ_1 is decreased or the spin relaxation time T_1 is increased with respect to their values at 1.49 eV. At high energy, as seen from the inset which shows the spectral dependences of τ_{1s} and of T_1, the polarization increase is caused by an increase of T_1 from 1.5 ns at 1.48 eV to about 3 ns at 1.50 eV, while τ_1 weakly depends on energy. This increase is caused by the reduced Coulomb interaction of energetic electrons with holes, which reduces the efficiency of spin relaxation. Below 1.49 eV, the increased polarization must be caused by the increase of T_1, which dominates the opposite effect of the increase of τ_1. In spite of the relatively

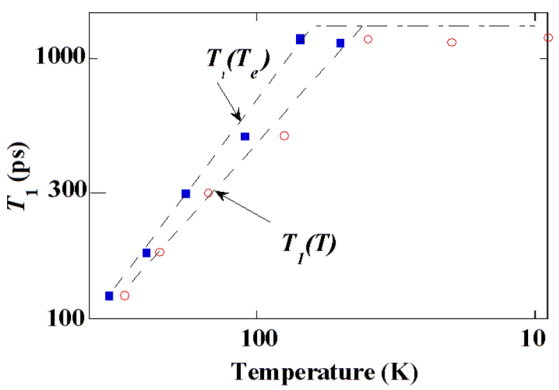

FIG. 7. Dependence of the spin relaxation time T_1 as a function of the lattice temperature T and of the temperature of the photoelectron gas T_e. At high temperature, these dependences follow a power law, of exponents 1.16 and of 1.41, respectively. The latter exponent is close to the one predicted by the Bir Aronov Pikus model for relaxation by exchange with holes.

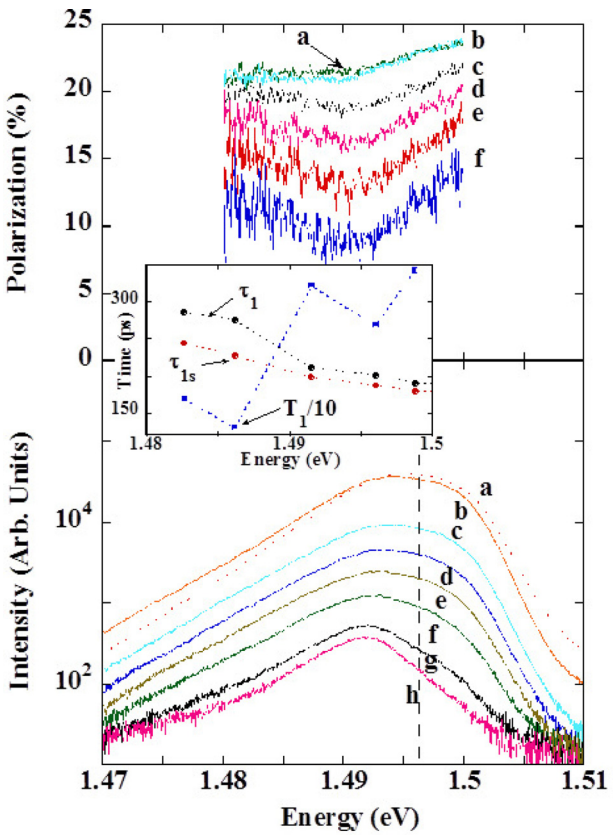

FIG. 8. Energy-dependent TRPL at 10 K. The bottom panel shows the luminescence spectra at 10 K taken after a delay of 50 ps, corresponding to the maximum of the signal (a), 150 ps (b), 400 ps (c), 550 ps (d), 700 ps (e), 900 ps (f), 1300 ps (g), and 2000 ps (h) after the laser pulse. The top panel shows the corresponding light polarization spectra, where curves g and h have been omitted, as well as regions of poor signal-to-noise in the polarization spectra. The inset shows the energy dependences of τ_1, and τ_{1s}, extracted from the sum and difference transients according to Eq. (7) and of the resulting spin relaxation time T_1.

poor accuracy of the determination of T_1 in conditions of weak signal conditions, the increased value of T_1 near 1.48 eV is visible in the inset of Fig. 8. This decrease of the spin relaxation efficiency of localized electrons by exchange with holes is viewed as a consequence of the smaller overlap of their wavefunctions, which decreases the electron-hole collision probability.

V. CONCLUSION

The charge and spin dynamics of p^+ GaAs have been investigated as a function of temperature using a novel method. This technique consists in combining spatially and time-resolved luminescence investigations. These two complementary, all optical, techniques, although quite different from an experimental point of view, have close conceptual analogies since corresponding signals are the solutions of very similar diffusion equations. The time decay of the signal exhibits well-defined exponential modes which are isolated using an inverse Laplace transform method. The spatial luminescence profile for a tightly focussed light excitation, given by an analytical resolution of the diffusion equation, is also predicted to exhibit spatial modes. The combination of these two techniques gives the charge and spin diffusion constants as well as bulk recombination time and spin relaxation time.

This method is applied between 9 K and 300 K to p^+ GaAs thin films, covered by a natural oxide layer. The diffusion constant is found to decrease slightly upon increasing temperature. The characteristic times τ_1 and τ_2 of the TRPL modes increase with temperature, implying that the surface recombination velocity increase is masked by the decrease of the efficiency of bulk recombination. The spin relaxation time T_1 decreases with increasing temperature and its dependence as a function of the temperature T_e of the electron gas follows the $T_e^{3/2}$ law characteristic of relaxation by exchange coupling with holes.

ACKNOWLEDGMENTS

The help of D. Lagarde on TRPL experiments is kindly acknowledged. One of us (F.C.) is grateful to CONICYT Grant Becas Chile for supporting his work.

APPENDIX: SOLUTION OF THE DIFFUSION EQUATION

The general method for solution of the diffusion equation, Eq. (2), is common to TRPL and μPL and consists in searching for a linear combination of the eigenfunctions $u_m(z)$ of the Laplace operator with time-dependent coefficients. These eigenfunctions, satisfying $\Delta u_m(z) + \lambda_m u_m(z) = 0$ as well as the boundary conditions, are

$$u_m(z) = \beta_m \left[\sin(v_m)\right]^{-1} \sin\left(\frac{\theta_m z}{d} + v_m\right), \tag{A1}$$

where θ_m is given by Eq. (6). Here, $v_m = \mathrm{Arctan}(\gamma_m/\theta_m)$ and the normalization factor β_m is given by

$$\frac{2}{d\beta_m^2} = 1 - \frac{\sin(2\theta_m)}{2\theta_m} + \gamma^{-1}[1 - \cos(2\theta_m)] + (\theta_m/\gamma)^2\left[1 + \frac{\cos(2\theta_m)}{2\theta_m}\right]. \tag{A2}$$

The corresponding eigenvalue is given by $\lambda_m = (\theta_m/d)^2$ and the eigenfunctions are such that $\int_0^d u_m(z)u_{m'}(z)dz = \delta_{mm'}$, where $\delta_{mm'}$ is the Kronecker symbol.

For TRPL, we search for a solution of the type $\sum_m u_m(z)c_m(t)$, where $c_m(t)$ can be a function of time. Inserting this expression into Eq. (2), multiplying by $u_m(z)$ and integrating over z, we find that the general solution of the time-resolved diffusion equation is given by Eq. (7) where the characteristic times τ_m of the various modes are given by Eq. (5), and

$$c_m = \int_0^t e^{t'/\tau_m}\left[\int_0^d g_{TR}(z,t')u_m(z)dz\right]dt'. \tag{A3}$$

For t' larger than the time for thermalization, $\int_0^d g_{TR}(z,t')u_m(z)dz$ is zero so that for t larger than this same time, c_m converges to a value which depends on the details of thermalization. In the case, considered in Sec. II B, where thermalization effects are neglected, one has $g_{TR}(z,t) = \alpha\delta(t)e^{-\alpha z}$ in Eq. (2). The amplitudes c_m, found by imposing that, at $t=0$, $n(z,0) = n_0 e^{-\alpha z}$, are given by $c_m = n_0 c_m^0$ where

$$c_m^0 = \beta_m^2 A_m(\alpha)A_m(\alpha_l) \tag{A4}$$

and

$$A_m(x) = [x^2 + (\theta_m/d)^2]^{-1} \times \left\{\theta_m(1/d + x/\gamma) - e^{xd}\left[\cos(\theta_m)\left[\frac{\theta_m}{d} + \frac{x}{\gamma}\right] + \sin(\theta_m)\left[x - \frac{\theta_m^2}{\gamma d}\right]\right]\right\} \tag{A5}$$

is the amplitude of the projection of e^{-xz} on $u_m(z)$. Note that the functions c_m defined by Eq. (A3) differ from their values of Eq. (A5) even at long times, provided the time τ_m is not very long as compared with the characteristic time τ_{th} of thermalization. This can be shown in the simple case where thermalization is characterized by a single exponential of time τ_{th} and assuming that the photoelectron concentration profile as a function of depth does not change during thermalization. Taking $g_{TR}(z,t) = \alpha\tau_{th}^{-1}e^{-\alpha z - t/\tau_{th}}$, one finds

$$I_{\mathrm{TR}}(t) = C\sum_m \frac{c_m^0}{1 - \tau_{th}/\tau_m}\left[e^{-t/\tau_m} - e^{-t/\tau_{th}}\right]. \tag{A6}$$

The effective amplitude $c_m^0/(1 - \tau_{th}/\tau_m)$ of mode m can differ significantly from c_m^0 for high order modes for which τ_m is comparable with τ_{th}.

The same method can be applied to find the solution of the diffusion equation for μPL and gives Eq. (8). This solution also uses the amplitude of the projections of $e^{-\alpha z}$ and of $e^{-\alpha_l z}$ on $u_m(z)$ so that the same coefficient c_m^0 is used

for spatial and time modes. Fig. 9 shows the luminescence profiles corresponding to the first three spatial modes, calculated using $S'=0$. For a low value of $S=10^4$ cm/s (bottom panel), the spatial mode of order 1 is strongly dominant at all distances. This is expected from Fig. 3, which shows that the higher order modes are negligible at low γ. In the opposite case where $S=10^7$ cm/s (top panel of Fig. 9), one finds $c_2^0/c_1^0=0.4$ and $c_3^0/c_1^0=0.17$ so that the second order mode is only negligible with respect to the first order one at distances larger than about 2 μm. It is concluded that higher order modes do not prevent the determination of L_1.

Note finally that, for μPL, the diffusion equation also has an analytical solution, obtained by using a similar approach as Ref. 24. The in-plane Fourier transform $\hat{G}(\xi,z)$ of the Green's function $G(r,\,z)$, which is the response to a Dirac excitation at the point $r=0$, $z=z'$, satisfies an ordinary differential equation with respect to z. One obtains

$$G(\xi,z-z')=\frac{\tau}{4\pi L\kappa}\left[e^{-\kappa|z^*-z'^*|}+\frac{\kappa-\gamma}{\kappa+\gamma}e^{-\kappa(z^*+z'^*)}+\frac{2(\kappa-\gamma')(\kappa\cosh\kappa z^*+\gamma\sinh\kappa z^*)(\kappa\cosh\kappa z'^*+\gamma\sinh\kappa z'^*)}{e^{\kappa d}(\kappa+\gamma)\left[(\gamma\gamma'+\kappa^2)\sinh\kappa d+\kappa(\gamma+\gamma')\cosh\kappa d\right]}\right], \tag{A7}$$

where $\kappa=\sqrt{1+\xi^2L^2}$, $z^*=z/L$, and $z'^*=z'/L$. The photoelectron concentration is then given by

$$n(r,z)=2\pi\int_0^\infty \xi\varphi(\xi)J_0(\xi r)d\xi\int_0^d e^{-\alpha^* z'}G(\xi,z-z')dz', \tag{A8}$$

where $\varphi(\xi)\propto e^{-\xi^2\sigma^{*2}/4}$ is the Fourier transform of the excitation profile and $J_0(\xi r)$ is a Bessel function of the first kind.

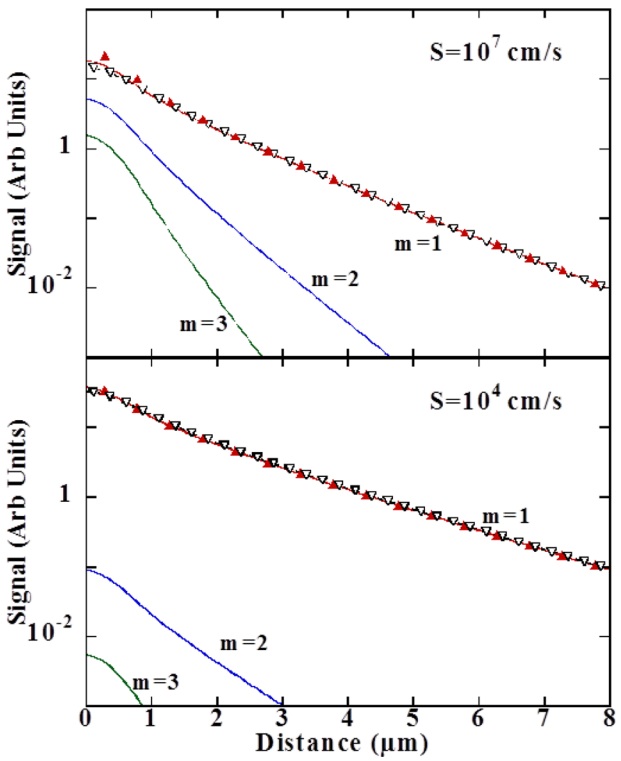

FIG. 9. The solid lines show the concentration profiles corresponding to the first 3 spatial modes, calculated using Eq. (8) for $D=100$ cm^2/s, $\tau=300$ ps, $\sigma=0.5$ μm, $\alpha_l=0$, and $S'=0$. S is taken equal to 10^4 cm/s in the bottom panel and 10^7 cm/s in the top panel. The sums of these modes are shown by full triangles and are in good agreement with the profiles, shown by open triangles, calculated using Eq. (A8) and using $S=S'=0$ and $L=L_1$. The effect of modes of $m>1$ is negligible for $S=10^4$ cm/s, and only slightly affects the profile for $S=10^7$ cm/s for $r<1$ μm.

Because of its integral form, this solution does not allow us to physically discuss the shape of the luminescence profile in the same way as Eq. (8) and requires the knowledge of three parameters which are S, S', and L. However, its main interest is that it is possible to take $S=S'=0$ and $L=L_1$, which is equivalent to take in Eq. (8) all L_m equal to L_1. Shown by open triangles in Fig. 9 is, for both values of S, the profile calculated using Eq. (A8). In the bottom panel, the result closely corresponds to the first spatial mode. This is expected because higher order modes are negligible. In the top panel, the result only slightly differs from the sum of the first three modes near the center and closely corresponds to this sum for $r>1$ μm. It is concluded that Eq. (A8) is in all cases a good approximation to the profile using the only parameter L_1.

[1]J. R. Lowney and H. S. Bennett, J. Appl. Phys. **69**, 7102 (1991).
[2]M. L. Lovejoy, M. R. Melloch, and M. S. Lundstrom, Appl. Phys. Lett. **67**, 1101 (1995).
[3]K. Beyzavi, K. Lee, D. M. Kim, M. I. Nathan, K. Wrenner, and S. L. Wright, Appl. Phys. Lett. **58**, 1268 (1991).
[4]A. R. Cameron, P. Riblet, and A. Miller, Phys. Rev. Lett. **76**, 4793 (1996).
[5]R. K. Ahrenkiel, *Semiconductors and Semimetals* (Academic, New York, 1993), Vol. 39.
[6]M. Boulou and D. Bois, J. Appl. Phys. **48**, 4713 (1977).
[7]H. Maaref, J. Barreau, M. Brousseau, J. Colet, and J. Mazzaschi, Solid State Commun. **25**, 601 (1978).
[8]R. Ahrenkiel and S. Johnston, Sol. Energy Mater. Sol. Cells **93**, 645 (2009).
[9]Y. Ogita, J. Appl. Phys. **79**, 6954 (1996).
[10]G. W. 't Hooft and C. van Opdorp, J. Appl. Phys. **60**, 1065 (1986).
[11]R. J. Nelson and R. G. Sobers, J. Appl. Phys. **49**, 6103 (1978).
[12]J. M. Olson, R. K. Ahrenkiel, D. J. Duniavy, B. Keyes, and A. E. Kibbler, Appl. Phys. Lett. **55**, 1208 (1989).
[13]R. J. Seymour, M. R. Junnarkar, and R. R. Alfano, Solid State Commun. **41**, 657 (1982).
[14]H. Horinaka, D. Ono, W. Zhen, K. Wada, Y. Cho, Y. Hayashi, T. Nakanishi, S. Okumi, H. Aoyagi, T. Saka *et al.*, Jpn. J. Appl. Phys., Part 1 **34**, 6444 (1995).
[15]R. Shinohara, K. Yamaguchi, H. Hirota, Y. Suzuki, T. Manago, H. Akinaga, T. Kuroda, and F. Minami, Jpn. J. Appl. Phys., Part 1 **39**, 7093 (2000).
[16]G. G. Gilliland, D. J. Wolford, T. F. Kuech, J. A. Bradley, and H. P. Hjalmarson, J. Appl. Phys. **73**, 8386 (1993).
[17]I. Favorskiy, D. Vu, E. Peytavit, S. Arscott, D. Paget, and A. C. H. Rowe, Rev. Sci. Instrum. **81**, 103902 (2010).

[18]T. T. Zhang, P. Barate, C. T. Nguyen, A. Ballochi, T. Amand, P. Renucci, H. Carrere, B. Urbaszek, and X. Marie, Phys. Rev. B **87**, 041201(R) (2013).
[19]D. Paget, F. Cadiz, A. C. H. Rowe, F. Moreau, S. Arscott, and E. Peytavit, J. Appl. Phys. **111**, 123720 (2012).
[20]F. Cadiz, D. Paget, and A. C. H. Rowe, Phys. Rev. Lett. **111**, 246601 (2013).
[21]I. D'Amico and G. Vignale, Phys. Rev. B **65**, 085109 (2002).
[22]H. S. Carlslaw and J. C. Jaeger, *Conduction of Heat in Solids* (Oxford University Press, 1966).
[23]The same calculation performed for a realistic value of $\alpha_l = 0.3$ shows that, for $\gamma > 1$, reabsorption is equivalent, as expected, to increase the importance of surface recombination. Conversely, at very low γ, photons originating from the recombination of secondary electrons are not included in the PL intensity, which leads to an artificially high γ. Thus, care should be taken in using the usual equation Eq. (1) for calculating the luminescence intensity at low γ.
[24]M. Duran, I. Muga, and J. C. Nedelec, C. R. Acad. Sci. Paris, Ser. I **341**, 561 (2005).
[25]L. Venkataramanan, Y. Q. Song, and M. D. Hurlimann, IEEE Trans. Signal Process. **50**, 1017 (2002).
[26]W. P. Dumke, Phys. Rev. **132**, 1998 (1963).
[27]K. Leo and J. Collet, Phys. Rev. B **44**, 5535 (1991).
[28]G. Marchetti, M. Hodgson, J. McHugh, R. Chantrell, and I. D'amico, Materials **7**, 2795 (2014).
[29]J.-N. Chazalviel, *Coulomb Screening by Mobiles Charges: Applications to Material Science, Chemistry and Biology* (Springer, 1999).
[30]R. J. Seymour and R. R. Alfano, Appl. Phys. Lett. **37**, 231 (1980).
[31]A similar approach in principle enables to determine the spin diffusion constant using the spin-polarized TRPL and μPL. However, such method is relatively imprecise and will not be discussed here.
[32]Since the TRPL results corresponding to the μPL ones at 15 K were obtained at a slightly higher temperature of 20 K, the value of D was modified, by a value smaller than the uncertainty, using an interpolation with the data obtained at 40 K.
[33]F. Cadiz, D. Paget, A. C. H. Rowe, V. L. Berkovits, V. P. Ulin, S. Arscott, and E. Peytavit, J. Appl. Phys. **114**, 103711 (2013).
[34]K. Zerrouati, F. Fabre, G. Bacquet, J. Bandet, J. Frandon, G. Lampel, and D. Paget, Phys. Rev. B **37**, 1334 (1988).
[35]Z. I. Alferov, V. M. Andreev, D. Z. Garbuzov, and M. K. Trukan, in Proceedings of the Eleventh International Conference on the Physics of Semiconductors, Warsaw (PWN-Polish Scientific, Warsaw, 1972).
[36]S. I. Kim, C. S. Son, S. W. Chung, Y. K. Park, E. K. Kim, and S. K. Min, Thin Solid Films **310**, 63 (1997).